AGU PUBLICATIONS

Water Resources Research

RESEARCH ARTICLE
10.1002/2013WR014955

Special Section:
Eco-hydrology of Semiarid Environments: Confronting Mathematical Models with Ecosystem Complexity

How will increases in rainfall intensity affect semiarid ecosystems?

Koen Siteur[1], Maarten B. Eppinga[1], Derek Karssenberg[2], Mara Baudena[1], Marc F.P. Bierkens[2], and Max Rietkerk[1]

[1]Department of Environmental Sciences, Faculty of Geosciences, Copernicus Institute of Sustainable Development, Utrecht University, Utrecht, Netherlands, [2] Department of Physical Geography, Faculty of Geosciences, Utrecht University, Utrecht, Netherlands

Key Points:
- Rainfall intensity controls patterning and the resilience of arid ecosystems
- Both an increase and decrease in rainfall intensity can trigger desertification
- In line with observations, three types of rain events were identified in our model

Correspondence to:
K. Siteur,
k.siteur@uu.nl

Citation:
Siteur, K., M. B. Eppinga, D. Karssenberg, M. Baudena, M. F. P. Bierkens, and M. Rietkerk (2014), How will increases in rainfall intensity affect semiarid ecosystems?, *Water Resour. Res.*, *50*, 5980–6001, doi:10.1002/2013WR014955.

Received 28 OCT 2013
Accepted 25 JUN 2014
Accepted article online 27 JUN 2014
Published online 17 JUL 2014

Abstract Model studies suggest that semiarid ecosystems with patterned vegetation can respond in a nonlinear way to climate change. This means that gradual changes can result in a rapid transition to a desertified state. Previous model studies focused on the response of patterned semiarid ecosystems to changes in mean annual rainfall. The intensity of rain events, however, is projected to change as well in the coming decades. In this paper, we study the effect of changes in rainfall intensity on the functioning of patterned semiarid ecosystems with a spatially explicit model that captures rainwater partitioning and runoff-runon processes with simple event-based process descriptions. Analytical and numerical analyses of the model revealed that rainfall intensity is a key parameter in explaining patterning of vegetation in semiarid ecosystems as low mean rainfall intensities do not allow for vegetation patterning to occur. Surprisingly, we found that, for a constant annual rainfall rate, both an increase and a decrease in mean rainfall intensity can trigger desertification. An increase negatively affects productivity as a greater fraction of the rainwater is lost as runoff. This can result in a shift to a bare desert state only if the mean rainfall intensity exceeds the infiltration capacity of bare soil. On the other hand, a decrease in mean rainfall intensity leads to an increased fraction of rainwater infiltrating in bare soils, remaining unavailable to plants. Our findings suggest that considering rainfall intensity as a variable may help in assessing the proximity to regime shifts in patterned semiarid ecosystems and that monitoring losses of resource through runoff and bare soil infiltration could be used to determine ecosystem resilience.

1. Introduction

In semiarid environments, plants can locally modulate their environment in a way that enables better access to resources, such as nutrients and water, thereby acting as so-called ecosystem engineers [*Jones et al*., 1994]. If the positive effect of plants on enhanced access to resources outweighs the negative effect of increased resource uptake, this may result in a positive feedback loop: an increase in plant biomass results in higher resource availability and consequently enhanced plant growth. This mechanism allows high plant densities to be maintained under harsher conditions, but it can also result in bistability (or multistability) of the ecosystem [*Rietkerk et al*., 1997], meaning that alternative stable system states exist under a given range of external conditions [*Lewontin*, 1969]. Changes in external conditions can alter the stability and the number of system states. In the case of semiarid ecosystems, increasing grazing pressure or decreasing resource input may push the system over a critical threshold, resulting in a sudden critical transition from a vegetated state to a bare state [*Noy-Meir*, 1975; *Rietkerk et al*., 1997]. As such regime shifts are accompanied by significant and irreversible losses in biological productivity, they are often related to the process of desertification [e.g., *Kéfi et al*., 2007; *Von Hardenberg et al*., 2001]. Note that formal definitions of desertification are more complex and include changes in soil resources, soil geochemistry, and vegetation composition as pointed out by *Schlesinger et al*. [1990] and *D'Odorico et al*. [2013].

Although it is generally hard to determine whether ecosystems will indeed respond in such a nonlinear way to changing environmental conditions, model studies show that particular spatially periodic patterns may be used as indicator for alternative stability [*Rietkerk et al*., 2004; *Kéfi et al*., 2010]. This is the case if local facilitative interactions, responsible for nonlinear system behavior [*DeAngelis et al*., 1980], are linked to distal competitive interactions that are responsible for pattern formation [*Gierer and Meinhardt*, 1972; *Rietkerk and van de Koppel*, 2008]. In semiarid ecosystems such a link between local facilitative and distal competitive

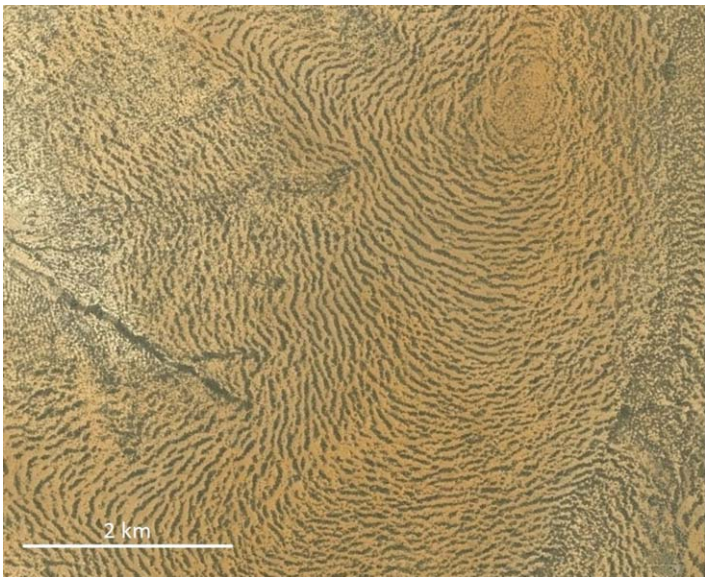

Figure 1. Periodically banded vegetation in Sudan (11°17′N, 28°13′E, mean annual precipitation: 450 mm yr^{-1}) [*Deblauwe et al*., 2008]. ©2013 Google Earth. ©2013 Cnes/Spot Image.

interactions exists and yields so-called scale-dependent feedbacks [*Rietkerk and van de Koppel*, 2008]. More specifically, in these ecosystems, plants can locally enhance the infiltration capacity of a soil by preventing crust formation and changing the soil structure. On sloped terrain, surface water accumulates on the barren or sparsely vegetated impenetrable soils during intense rain events, and flows downhill to the more densely vegetated soils where it can infiltrate, resulting in increased productivity. The depletion of surface water by vegetation uphill on the other hand has a negative effect on infiltration and plant growth downhill. This particular scale-dependent feedback, referred to as the resource concentration mechanism [*Rietkerk et al*., 2004], can result in the formation of regularly spaced vegetation bands perpendicular to the slope separated by interbands of bare soil (Figure 1) [*Klausmeier*, 1999; *Rietkerk et al*., 2002].

A large body of spatially explicit mechanistic models have been published that describe pattern formation in semiarid ecosystems [see, for example, *Lefever and Lejeune*, 1997; *Klausmeier*, 1999; *Von Hardenberg et al*., 2001; *Rietkerk et al*., 2002; *Gilad et al*., 2004; and for a review, *Borgogno et al*., 2009]. These models were successful in identifying possible mechanisms driving pattern formation in semiarid ecosystems, such as the resource concentration mechanism, and provided insights regarding the nonlinear response of these systems when subject to gradual changes in mean annual rainfall.

Changes in annual and seasonal rainfall volumes in arid and semiarid regions, as projected by global climate models, are, however, subject to much uncertainty. Projections of changes in rainfall intensity in contrast, show strong trends [*Tebaldi et al*., 2006; *Solomon et al*., 2007]. For the Sahel region and the Horn of Africa, for example, a majority of the global climate models predicts significant elevations in rainfall intensity at the end of this century with respect to the 1980s and 1990s [*Tebaldi et al*. 2006; *Solomon et al*. 2007].

Model studies show that spatiotemporal patterns in infiltration and soil moisture are to a large extent determined by rainfall intensity and storm size. *Rodriguez-Iturbe et al*. [1999] show that average soil moisture increases with rainfall depth, and that there is bell-shaped relation between rainfall depth and variance. A study by *Thompson et al*. [2011] shows that the spatial infiltration patterns in patchy arid ecosystems are strongly controlled by rainfall intensity. During intense events, enhanced infiltration occurs for a large portion of vegetated sites, whereas during low intensity events increased recharge occurs only at the edges of vegetation patches. Although hydrological models show that rainfall intensity plays a key role in rainwater partitioning and lateral surface water redistribution, it is unknown if and exactly how the projected changes in rainfall intensity are going to affect the productivity and functioning of patterned semiarid ecosystems.

Modeling the effect of changes in rainfall intensity on these ecosystems requires the coupling of processes that act on the time scale of a single rain event with processes, such as plant growth, that act on much longer time scales. The current spatially explicit models mostly capture rainfall in a continuous manner, and thereby they do not explicitly deal with this issue [*Konings et al*., 2011]. These models, as well the few that do consider rainfall to consist of separate events [*Kletter et al*., 2009; *Ursino and Contarini*, 2006], also assume infiltration to depend on surface water depth [e.g., *HilleRisLambers et al*., 2001; *Rietkerk et al*., 2002; *Gilad et al*., 2004; *Meron et al*., 2007], which is in contrast with conventional depth independent infiltration models [e.g., *Horton*, 1939; *Philip*, 1957]. The study by *Thompson et al*. [2011] shows that this assumption leads to

insensitivity of surface water redistribution to changes in rainfall intensity. The use of depth-dependent infiltration models may therefore underestimate the potential effects such changes may have on ecosystem functioning.

In this paper, we study the response of semiarid ecosystems to changes in rainfall intensity using a spatially explicit version of the water limitation model by *Rietkerk et al*. [1997] that is coupled with a hydrological hillslope model that explicitly describes depth independent infiltration and infiltration excess (Hortonian) runoff generation on an event basis with simple conditional rules. The full model acknowledges both the processes that operate on short temporal scales, such as rainwater partitioning and redistribution, as well as processes that operate on longer temporal scales, such as plant growth. Temporal upscaling of short-term processes and a minimalistic modeling approach enabled analytical analysis of the model.

2. Model Description

To study the role of rainfall intensity in semiarid ecosystems, we need to account for relatively slow processes that operate on long temporal scales, such as plant growth, as well as fast processes that operate on short temporal scales, such as the partitioning, and redistribution of rainwater during a rain event.

The slow long-term processes are modeled using a spatially extended version of the water-limitation model by *Rietkerk et al*. [1997], which describes the essential dynamics of plant density and available soil moisture in a minimalistic way [*Rietkerk*, 1998, pp. 4–5], thereby enabling detailed analytical analysis. Rainwater partitioning and the runoff-runon processes are fast short-term processes that are modeled with event-based descriptions in the form of simple conditional rules. Temporal upscaling of the obtained infiltration rates yields a continuous formulation for infiltration, which is then used in the spatially extended version of the water-limitation model by *Rietkerk et al*. [1997].

In sections 2.1 and 2.2, we will describe the water-limitation model. In section 2.3, infiltration for uniform system states will be discussed and in section 2.4, we account for spatial heterogeneity by including runoff-runon processes. The mechanism governing spatial patterning in this model is the resource concentration mechanism mentioned earlier; however, spatial feedbacks in our model differ from previous models because of the alternative modeling approach, as we will briefly discuss in section 2.5.

2.1. Soil Moisture Dynamics

Soil moisture dynamics comprise infiltration, plant uptake, soil evaporation and percolation losses, and lateral soil water movement. The change in available soil water W (mm) over time t (year) at location x (m) on the one-dimensional hillslope is modeled with equation (1):

$$\frac{\partial W}{\partial t} = i_{ag} - u\frac{W}{W+k}P - rW + d_W\frac{\partial^2 W}{\partial x^2} \tag{1}$$

Here i_{ag} is the mean aggregated infiltration rate of water into the soil (mm yr^{-1}), further discussed in subsections 2.3 and 2.4. The second term represents the uptake of water by plants, which is assumed to depend on local plant density. Here u is the maximum specific soil water uptake (mm m^2 g^{-1} yr^{-1}), P is the plant density (g m^{-2}), and k is the half saturation constant of soil water uptake (mm). Losses in available soil water are modeled with the third term, in which r is the specific soil water loss due to soil evaporation and percolation (yr^{-1}). The last term represents soil water movement, with d_W being the diffusion rate of soil water (m^2 yr^{-1}) and x space (m). Note that soil water is assumed to diffuse in a linear way and that also percolation and evaporation losses depend linearly on soil water availability [*Rietkerk et al*., 2002].

2.2. Plant Growth

In the model, plant dynamics is captured by growth, mortality and grazing, and plant dispersion. The change in plant density P is given by equation (2):

$$\frac{\partial P}{\partial t} = cu\frac{W}{W+k}P - mP + d_P\frac{\partial^2 P}{\partial x^2} \tag{2}$$

The first term represents plant growth, which is linearly related to water uptake. Here c is the conversion of water uptake by plants to plant growth (g mm^{-1} m^{-2}). The second term covers both mortality and grazing losses, with m being the specific plant loss due to mortality and herbivory (yr^{-1}). Plant dispersal is modeled with the last term. Here d_P is the dispersion rate of plants (m^2 yr^{-1}).

2.3. Infiltration Neglecting Runon (for Uniform Case and Interbands)

In this section, we will solely consider the partitioning of rainwater into infiltration and runoff, and neglect runon, which we define as the infiltration of runoff generated uphill. This assumption is valid for uniform system states and interbands, as we will explain later.

The partitioning of rainwater into infiltration and runoff differs per rain event. In this model, the infiltration rate during a given event i_{ev} (mm h^{-1}) is limited by either the infiltration capacity of the soil i_{cap} (mm h^{-1}) or the intensity of the rain event p_{ev} (mm h^{-1}), which is considered to be a random variable. In the former case not all rainwater infiltrates, but part is lost in the form of runoff. The infiltration rate i_{ev} for a rain event with intensity p_{ev} in a soil with infiltration capacity i_{cap} is given by:

$$i_{ev}(x, p_{ev}) = \begin{cases} p_{ev} & \text{if} \quad p_{ev} < i_{cap}(x) \\ i_{cap}(x) & \quad\quad p_{ev} \geq i_{cap}(x) \end{cases} \tag{3}$$

By using this relationship, we assume steady state infiltration conditions [*Karssenberg*, 2006]. In other words, during the rain event i_{ev}, p_{ev}, and i_{cap} are constant over time. For soils with high sorptivity, this time independency results in underestimation of infiltration during short events and overestimation during long events. On average, however, the error will be negligible provided that rainfall intensity and event duration are mutually independent. Notice that, although we consider infiltration to be independent of surface water depth [*Horton*, 1939; *Philip*, 1957], there may be situations, including soil cracking and crusting, in which surface water depth is important [*Dunne et al*., 1991; *Fox et al*., 1998; *Novak et al*., 2000].

The interarrival time between rain events is assumed to be sufficiently large, so that infiltration conditions, which are affected by antecedent soil moisture content, are similar for all events. With this assumption, we neglect possible interactions between storm events, which in allows analytical analysis of the model. Infiltration capacity i_{cap} increases with plant density P [*van Wijngaarden*, 1985; *Rietkerk et al*., 2000; *Thompson et al*., 2010a] and is modeled with equation (4):

$$i_{cap}(x) = i_0 + aP(x) \tag{4}$$

Here i_0 is the infiltration capacity of bare soil (mm h^{-1}), and a is the increase of infiltration capacity with plant density (mm m^2 h^{-1} g^{-1}).

We assume rainfall intensity p_{ev} to be an exponentially distributed random variable with mean $\mu_{p_{ev}}$ (mm h^{-1}) [*Hoogmoed*, 1981] that is uniform in space. Its probability density function is given by equation (5):

$$f(p_{ev}) = \frac{1}{\mu_{p_{ev}}} e^{-\frac{p_{ev}}{\mu_{p_{ev}}}} \tag{5}$$

The fact that p_{ev} is a random variable, makes i_{ev} a random variable (if $i_{cap} > 0$). In other words, the amount of water that infiltrates is different for each rain event. Although we consider infiltration to be a random process, the equilibrium analysis and model runs will be done using the expected value (or long-term average) of i_{ev}. Thereby we assume the response of vegetation to individual rain events is slow. Working with the expected infiltration rate makes the model deterministic and allows studying the system's equilibria and the effects of changes in mean rainfall intensity on the system. Note, however, that the obtained solutions for P and W presented in section 3 only approximate the expected values of P and W at first order. This

means that we neglect the effects of variance and higher order moments of infiltration rate on available soil water and plant productivity.

The expected infiltration rate $E(i_{ev})$ is obtained by summing the infiltration rates (equation (3)) over all possible event intensities ($p_{ev} > 0$) while multiplying with the probability of occurrence of the events (equation (5)). As shown in Appendix A this yields:

$$E(i_{ev}(x, p_{ev})) = \mu_{p_{ev}} \left(1 - e^{-\frac{i_{cap}(x)}{\mu_{p_{ev}}}}\right) \tag{6}$$

If we assume the arrival of rain events to be a Poisson process [*Bierkens and Puente*, 1990] and the events to have a mutually independent duration and intensity [*Hoogmoed*, 1981], then the mean rainfall rate aggregated over a period of time p_{ag} (mm yr^{-1}) is given by the product of the mean frequency of the events λ (yr^{-1}), the mean duration of an event τ (h), and the mean rainfall intensity $\mu_{p_{ev}}$ (mm h^{-1}). The aggregated infiltration rate $i_{ag}(x)$ (mm yr^{-1}), used in equation (1), can now be written as function of aggregated rainfall p_{ag}:

$$i_{ag}(x) = \lambda\tau E(i_{ev}(x, p_{ev})) = p_{ag} \frac{E(i_{ev}(x, p_{ev}))}{\mu_{p_{ev}}} = p_{ag} \left(1 - e^{-\frac{i_{cap}(x)}{\mu_{p_{ev}}}}\right) \tag{7}$$

Similar to infiltration in the model by *Rietkerk et al*. [1997], the aggregated infiltration rate $i_{ag}(x)$ increases asymptotically to p_{ag} for $P \to \infty$.

In this section, we neglected the infiltration of runoff produced uphill (runon). As mentioned, this assumption is valid under particular conditions. For example, if plant density and infiltration capacity are spatially homogeneous, runoff is produced if $i_{cap}(x)$ is exceeded ($p_{ev} > i_{cap}(x)$). However, if $p_{ev} > i_{cap}(x)$ and if $i_{cap}(x)$ is equal for all x, runoff will not infiltrate downhill as the maximum infiltration rate $i_{cap}(x)$ is already reached for all x. In the case, that $p_{ev} < i_{cap}(x)$, no runoff is generated at any x, and therefore runon can be neglected as well. If plant density is not uniform and infiltration capacity is spatially heterogeneous, still areas exist where runon does not occur and infiltration is approximated by equation (7), as will be discussed in section 2.5.

2.4. Infiltration Including Runon (Nonuniform Case)

In this section, we will continue with the approach of section 2.3, but now we include the infiltration of runoff produced uphill (runon). Runoff generation and its infiltration downhill are modeled similarly to *Karssenberg* [2006], with the difference that we use a spatially continuous formulation, which allows to calculate the expected infiltration rate as in the previous section. Runoff is generated where rainfall intensity p_{ev} exceeds infiltration capacity $i_{cap}(x)$ and is transported downhill. Again two cases can be distinguished: (1) Infiltration rate $i_{ev}(x)$ equals infiltration capacity $i_{cap}(x)$ in areas where runoff is generated (i.e., $p_{ev} > i_{cap}(x)$) and directly downhill of these areas due to runon. (2) In areas that do no receive surface water (e.g., due to depletion uphill) infiltration rate equals the rainfall intensity. A critical rainfall intensity $\tilde{p}_{ev}(x)$ separates the two cases (see Figure 2):

$$i_{ev}(x, p_{ev}) = \begin{cases} p_{ev} & \text{if} \quad p_{ev} < \tilde{p}_{ev}(x) \\ i_{cap}(x) & \quad\quad p_{ev} \geq \tilde{p}_{ev}(x) \end{cases} \tag{8}$$

The critical rainfall intensity $\tilde{p}_{ev}(x)$ in mm h^{-1} is the minimum rainfall intensity required for surface water to reach position x on the hillslope and can be derived as follows.

In order for surface water to reach site x, the cumulative rainfall intensity uphill of x needs to exceed the cumulative infiltration capacity uphill of x. The cumulative infiltration capacity $\hat{i}_{cap}$ (m mm h^{-1}) upslope of x increases with distance l (m) from x.

$$\hat{i}_{cap}(l, x) = \int_{x-l}^{x} (i_{cap}(x'))\mathrm{d}x' \tag{9}$$

Since rainfall is assumed to be spatially uniform, the cumulative rainfall intensity between $x - l$ and x, ($\hat{p}_{ev}$ in m mm h^{-1}) is independent of x and is given by:

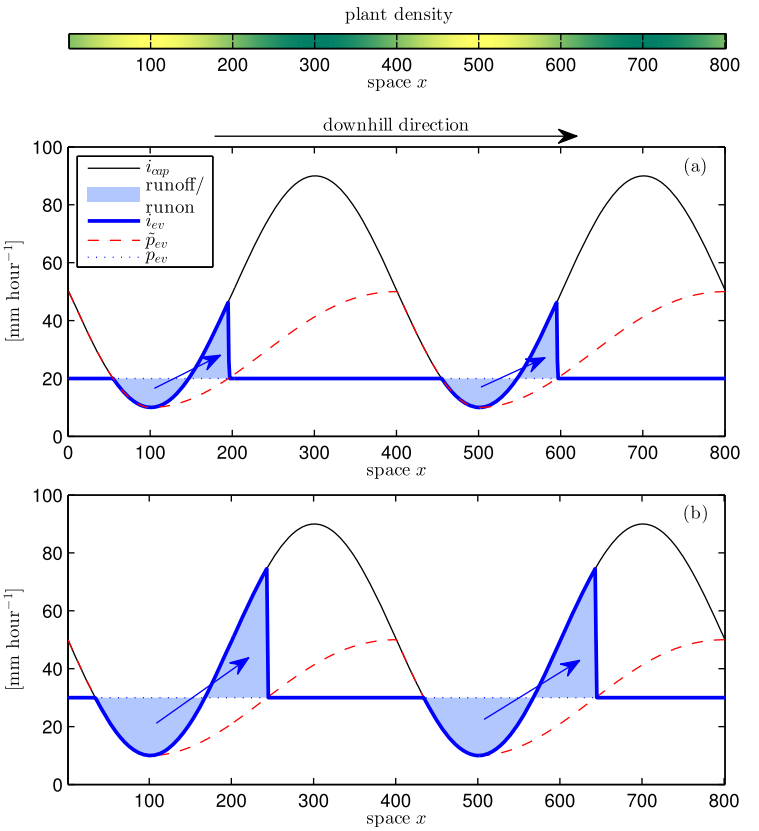

Figure 2. Infiltration capacity i_{cap}, critical rainfall intensity $\tilde{p}_{ev}$, and infiltration rates i_{ev} for rain events with intensities p_{ev} of (a) 20 mm h^{-1} and (b) 30 mm h^{-1} on a hillslope with an imposed periodic pattern in plant density (P ranges from 0 to 40 g m^{-2}). The critical rainfall intensity $\tilde{p}_{ev}$ is the minimum rainfall intensity required for a particular location on the hillslope to receive surface water. The arrows indicate how the generated runoff is relocated. For some areas on the hillslope, $\tilde{p}_{ev}(x)=i_{cap}(x)$. Notice that the amount of runon is equal to the amount of runoff that is generated and that surface water is transported further downhill during more intense rain events.

$$\hat{p}_{ev}(I,p_{ev})=Ip_{ev} \tag{10}$$

If $\hat{p}_{ev}(I,p_{ev})$ exceeds $\hat{i}_{cap}(I,x)$ for any positive value of I, then surface water reaches x. The critical rainfall intensity equals the minimum rainfall intensity for which $\hat{p}_{ev}(I,p_{ev})=\hat{i}_{cap}(I,x)$ for some value of I (with $I>0$). From equations (9) and (10) follows that the critical rainfall intensity is given by:

$$\tilde{p}_{ev}(x)=\min_{I>0}\left(\frac{\hat{i}_{cap}(I,x)}{I}\right) \tag{11}$$

Here min () takes the minimum value of a given function. Note that by allowing I to have any positive value, we assume the hillslope to have an infinite length. If I tends to zero, then $\frac{\hat{i}_{cap}(I,x)}{I}$ tends to $i_{cap}(x)$. Therefore, if the minimum in equation (11) is located at I close to zero, then $\tilde{p}_{ev}(x)=i_{cap}(x)$. This is the case for some areas on the hillslope depicted in Figure 2.

The expected infiltration rate E(i_{ev}) can again be obtained by summing the infiltration rates (equation (8)) over all possible event intensities ($p_{ev}>0$) while multiplying with the probability of occurrence of the events (equation (5)). As shown in Appendix A, this yields:

$$\mathrm{E}(i_{ev}(x,p_{ev}))=\mu_{p_{ev}}+(i_{cap}(x)-\tilde{p}_{ev}(x)-\mu_{p_{ev}})e^{-\frac{\tilde{p}_{ev}(x)}{\mu_{p_{ev}}}} \tag{12}$$

The aggregated infiltration rate $i_{ag}(x)$ (mm yr^{-1}) used in equation (1) now becomes:

$$i_{ag}(x) = p_{ag} + p_{ag}\left(\frac{i_{cap}(x) - \tilde{p}_{ev}(x)}{\mu_{p_{ev}}} - 1\right) e^{-\frac{\tilde{p}_{ev}(x)}{i_{p_{ev}}}} \quad (13)$$

The full model is described by equations (1), (2), and (13). In case of uniform infiltration conditions, $\tilde{p}_{ev} = i_{cap}$ meaning that equation (13) reduces to equation (7).

Infiltration and runoff/runon process are modeled in a simple parsimonious way. Notice, for example, that hillslope gradient is not a parameter in equation (13). This is because we assume instantaneous surface water redistribution: all runoff generated uphill infiltrates downhill as long as infiltration capacity is not met. Models that, besides spatial infiltration contrasts, also incorporate contrasts in surface roughness and resistance to flow, suggest that such sophisticated approaches are only required on terrains with a slope up to around 0.1% [*Thompson et al*., 2011]. This supports our simplified approach, as the banded patterns we aim to model can only be found on hillslopes with a gradient greater than 0.2–0.25% [*Valentin et al*., 1999; *Deblauwe et al*., 2011]. Finally, the spatial infiltration patterns depicted in Figure 2 are comparable, though less smooth, to those found by more advanced models [*Thompson et al*. 2011].

2.5. Competition for Surface Water and Spatial Feedbacks

The competition for surface water in this model is fundamentally different from other conceptual models that describe pattern formation in semiarid ecosystems [e.g., *HilleRisLambers et al*., 2001; *Rietkerk et al*., 2002; *Gilad et al*., 2004; *Meron et al*., 2007]. These models do not consider soils to have a finite capacity to take up water. Instead, infiltration rate is considered to be a function of surface water depth which is modeled as a separate state variable. Since surface water accumulates on the bare interbands and is depleted as it is transported through the vegetation bands, bare areas positively affect infiltration in downhill vegetated areas while vegetated areas have a negative effect on the infiltration rate in the bare interbands in these models (see Appendix B). The positive effect enables patterned states to exist under harsher conditions than would be the case if vegetation was uniformly distributed [*Rietkerk et al*., 2002; *Sherratt and Lord*, 2007], while the negative effect is responsible for the formation of patterns [*Gierer and Meinhardt*, 1972; *van de Koppel and Crain*, 2006; *Rietkerk and van de Koppel*, 2008] and explains why bare areas emerge when uniform cover is still possible (i.e., Turing instability).

In our model, the positive effect is still active: runoff is generated on the bare interbands if rainfall intensity exceeds the infiltration capacity of bare soil (i.e., $p_{ev} > i_0$) and feeds the vegetation bands where the infiltration capacity is higher. However, the negative effect of the vegetation bands on the interbands is absent: the infiltration in the interbands is not affected by uphill vegetation. This is because runoff is only generated if $p_{ev} > i_0$, meaning that bare areas receive surface water only if, due to local rainfall, infiltration already occurs with a maximum rate of infiltration capacity. Consequently, additional infiltration due to runon does not occur on bare soil, regardless of rainfall intensity or the depth of the surface water layer. This means that for these areas equation (13) reduces to equation (7), meaning that infiltration in the interbands is independent of infiltration capacity uphill.

Because of the absence of a negative effect of areas with high plant densities on areas with lower plant densities, the behavior of our model can be expected to differ from that of the mentioned conceptual models. This will be discussed in section 3.

2.6. Parametrization and Analysis

We implemented the model in MATLAB (version R2012a – 7.14.0.739; The MathWorks, Inc.). The partial differential equations are solved numerically using a time-explicit scheme with a constant time step Δt. A vector of n elements, with each element having a length of Δx, represents the one-dimensional hillslope.

The model can be analyzed along only one spatial dimension, as we assume all water to flow downhill and neglect the exchange of surface water perpendicular to the hillslope. In models that do consider the exchange of water in this direction found that vegetation bands may break up to form dashed patterns [*Von Hardenberg et al*., 2001], which can also be found on imagery [*Valentin et al*., 1999]. These patterns are not considered in our analysis.

In the model runs, equation (11) was evaluated for $0 < l \leq n\Delta x$ only. Following *Klausmeier* [1999], *Rietkerk et al*. [2002], *Lejeune et al*. [2004], *Gilad et al*. [2004], and *Sherratt and Lord* [2007], we run the model using

Table 1. Parameter Values, Units, and Meaning[a]

Parameter	Description	Value	Unit	References
k	Half saturation constant of soil water uptake	5	mm	*Rietkerk et al.* [2002]
u	Maximum specific water uptake	18	mm m^2 g^{-1} yr^{-1}	*Rietkerk et al.* [1997]
r	Specific soil water loss due to evaporation and percolation	36	yr^{-1}	*Rietkerk et al.* [1997]
m	Specific loss of plant density due to mortality and grazing	126	yr^{-1}	*Rietkerk et al.* [1997]
c	The conversion of water uptake by plants to plant growth	10	g mm^{-1} m^{-2}	*Rietkerk et al.* [1997]
d_P	Dispersion rate of plants	36	m^2 yr^{-1}	*Rietkerk et al.* [2002]
d_W	Diffusion rate of water	36	m^2 yr^{-1}	*Rietkerk et al.* [2002]
p_{ag}	Aggregated rainfall rate	600	mm yr^{-1}	*Rietkerk et al.* [2002]
$\mu_{p_{ev}}$	Mean intensity of the rain events	20	mm h^{-1}	*DeBlauwe et al.* [2008][b]
i_0	Infiltration capacity of bare soil	10	mm h^{-1}	*DeBlauwe et al.* [2008][b]
a	Increase of the infiltration capacity with plant density	2	mm m^2 h^{-1} g^{-1}	*DeBlauwe et al.* [2008][b]
Δt	Time step size	5×10^{-4}	year	
Δx	Cell length	0.2	m	
n	Number of elements	4000		

[a]These parameter values are used throughout this work, unless indicated differently.
[b]Parameters were calibrated to obtain patterns in a realistic rainfall range according to the mentioned study.

periodic boundary conditions. Thereby we minimize the boundary effects, such as deviating pattern orientation in proximity to ridges [*McGrath et al.*, 2012] and increasing pattern wavelength close to streams [*Penny et al.*, 2013], which makes our results independent of site-specific properties, such as topography. The use of periodic boundary conditions implies that we only consider the hillslope far from ridges and streams. Notice, however, that it does not imply that surface water cannot escape from the modeled hillslope: it is either depleted along the hillslope (as in Figure 2) or discarded once infiltration capacity is met along the entire hillslope.

We performed runs of the model to study the patterned steady states. The model runs were initiated with random peaks in plant density in a fraction of the elements. To study the existence of stable patterned steady states with a particular wavelength, the peaks in plant density were distributed in a periodic fashion.

If environmental conditions, such as mean rainfall intensity, change, patterned states may cease to exist. The parameter range for which patterns with a particular wavelength exist was obtained using the bisection method (or binary search method) [*Burden and Faires*, 2011].

We analytically derived the uniform steady states of the system (expressed in plant density and water availability), as well as a rainfall range for which (patterned) vegetation and a stable bare desert state coexist (as discussed in Appendices C and D). This information, combined with runs of the model, allowed to examine the response of the system to changes in aggregated rainfall rate p_{ag} and mean rainfall intensity $\mu_{p_{ev}}$. Table 1 gives an overview of the parameters used in the model.

3. Results

In this section, we first describe the competition for water and feedbacks in the model on a local scale (section 3.1) in order to understand the global behavior of the model (section 3.2). In section 3.3, we will then discuss how the model responds to changes in rainfall intensity.

3.1. Competition for Water Along the Hillslope

With the parameter values of Table 1, the model generates spatially periodic patterns in plant density along the hillslope (Figure 3a). These periodic vegetation bands migrate in uphill direction: colonization occurs directly uphill from the vegetation bands, while plant density slowly decays in the downhill part of the bands. This is in line with observations [*Worrall*, 1959; *Deblauwe et al.*, 2012] and modeling studies [*Klausmeier*, 1999], although fixed patterns have also been reported [*Thompson and Katul*, 2009; *Dunkerley*, 2013]. Available soil water is generally higher in the vegetation bands compared to the bare interbands; however, a small depression in soil water availability can be found in the downhill part of the vegetation bands (Figure 3b).

Figure 3c shows the infiltration capacity $i_{cap}(x)$ and critical rainfall intensity $\tilde{p}_{ev}(x)$ in space. Expected infiltration rates (equation (12)) are high if the critical rainfall intensity is low and infiltration capacity is high. The

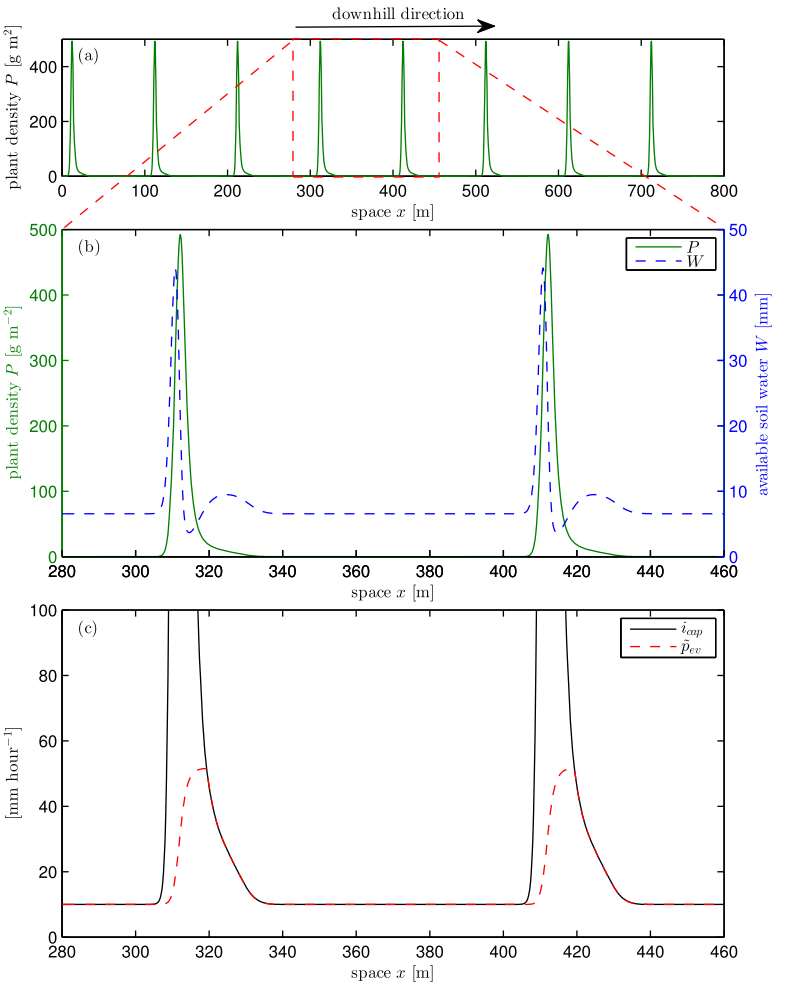

Figure 3. (a) Plant density P (g m^{-2}), (b) plant density P (g m^{-2}), and available soil water W (mm), and (c) infiltration capacity i_{cap} (mm h^{-1}) and critical rainfall intensity $\tilde{p}_{ev}$ (mm h^{-1}) along the hillslope. Notice that the minimum infiltration capacity on the hillslope—separating low intensity events from intermediate intensity events—is equal to the infiltration capacity of bare soil i_0. The maximum critical rainfall intensity on the hillslope—separating intermediate intensity events from high intensity events—equals the mean infiltration capacity of the hillslope. In Figure 3c, infiltration capacities above 100 mm h^{-1} were cut off. The peak infiltration capacity in the vegetation bands is about 1000 mm h^{-1}.

infiltration capacity increases linearly with plant density, following equation (4), and is therefore higher for more densely vegetated soils. In the vegetation bands, critical rainfall intensity increases in downhill direction. This means that a higher rainfall intensity is required for runon to occur in the downhill part as compared to the upslope part. In the interbands, the critical rainfall intensity is equal to the infiltration capacity. Here runon does not occur and the infiltration equation for the uniform case is valid (equation (6)).

When considering the effect of single rain events on the system, three types of rain events can be distinguished. *Low intensity events* have an intensity lower than the lowest infiltration capacity on the hillslope. These events do not trigger runoff generation, meaning that all rainwater infiltrates locally. Since the infiltration rate during such low intensity events is equal for every location along the hillslope, these events have a homogenizing effect on the spatial distribution of soil water and consequently vegetation. During *intermediate intensity events*, runoff is generated on the bare interbands and is transported to the vegetation bands where it is fully depleted. Since runon occurs in the uphill part of the vegetation bands and not in the downhill part, spatial competition occurs: uphill vegetation negatively affects infiltration downhill. Such negative spatial interactions are a requirement for regular pattern formation [*Gierer and Meinhardt*, 1972; *van de Koppel and Crain*, 2006; *Rietkerk and van de Koppel*, 2008]. During *high intensity events*, the rainfall intensity exceeds the maximum critical rainfall intensity on the hillslope. Now surface water reaches all locations on the hillslope and infiltration rate equals infiltration capacity for the entire hillslope. Plants may still

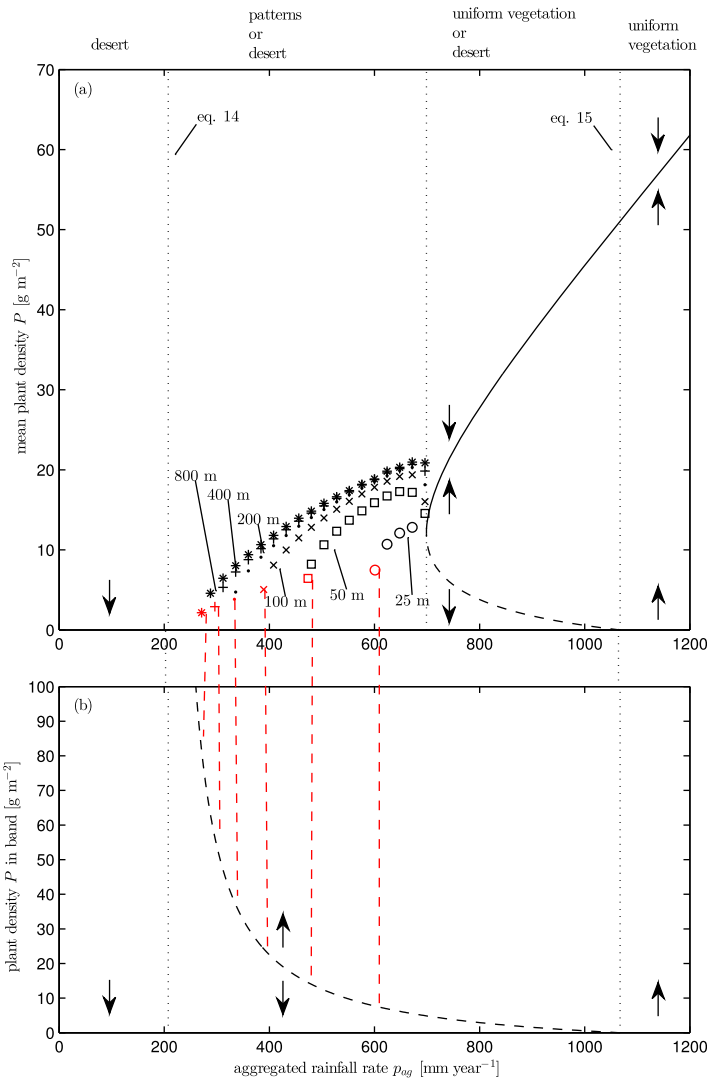

Figure 4. (a) The steady states of the system expressed in mean plant density P (g m^{-2}) plotted against aggregated rainfall rate p_{ag} (mm yr^{-1}). The solid and dashed lines depict the uniformly vegetated equilibria and can be written in terms of p_{ag} as shown in Appendix C. For this parameter setting, a stable uniform bare state exists for $p_{ag} < 1070$ mm yr^{-1} (equation (15)). The markers show the mean plant density for patterned states with different wavelengths obtained with runs of the model. The red markers are obtained using the bisection method and depict the mean plant density at which the stable patterned states cease to exist. (b) The dashed line shows the minimum plant density in a vegetation band required for plants to grow and ultimately sustain themselves (see Appendix C for a derivation). For $p_{ag} < 210$ mm yr^{-1} (equation (14)), infinite plant density is required to accomplish this. The arrows in Figures 4a and 4b indicate whether plant density increases or decreases if the system is out of equilibrium.

benefit from runoff produced uphill; however, since surface water is not fully depleted on its way through the vegetation bands spatial competition does not occur. In addition, not all generated runoff is able to infiltrate downhill, meaning that some water flows through the vegetation bands and is eventually lost from the system.

The categorization of rain events as described above helps in understanding the response of the system when subject to changes in mean rainfall intensity, as discussed in section 3.3.

3.2. Alternative Stable System States

Apart from the patterned state discussed so far, uniformly vegetated states and/or a bare desert state exist depending on parameter setting. Figure 4a shows a bifurcation diagram with aggregated rainfall p_{ag} as bifurcation parameter and with a constant mean rainfall intensity $\mu_{p_{ev}}$. For high rainfall values, only a uniformly vegetated state is stable and for very low rainfall values only a stable bare desert state exists. For intermediate aggregated rainfall values, the system has alternative stable states: stable patterned states or a stable uniformly vegetated state coexist with a stable bare state.

Notice that multiple stable patterned states with different pattern wavelengths can exist for a given parameter configuration. For high wavelength patterns, the plant density in the vegetation bands is higher compared to low wavelength patterns (see Figure 5). This is because high wavelengths come with a greater interband area, which enables plants to harvest more surface water [*Yizhaq et al.*, 2005]. We found that the plant density in the vegetation bands needs to be higher than a certain threshold value in order for plants to grow and ultimately sustain themselves. This minimum plant density depends on aggregated rainfall rate p_{ag} as shown in Figure 4b (see Appendix C for a derivation). Since plant density in the vegetation bands increases with wavelength and because the minimum required plant density increases with aridity (Figure 4b), high wavelength patterns can persist under more arid conditions. As rainfall decreases, an adaptation of pattern wavelength occurs once a patterned state

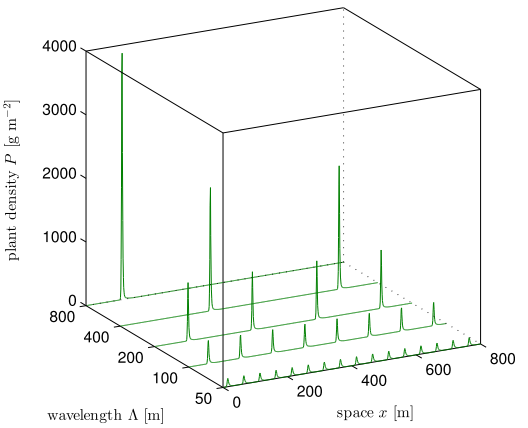

Figure 5. Patterns in plant density P with different wavelengths Λ but with a fixed parameter setting (Table 1). Notice that the plant density in the vegetation bands increases with wavelength, enabling high wavelength patterns to persist in drier climates (Figure 4b).

with a certain wavelength can no longer be sustained [*Sherratt*, 2013]. At low rainfall values ($p_{ag} < 210$ mm yr^{-1} for the current parameter setting), the minimum required plant density tends to infinity. Here stable patterned system states cannot exist. For our model, we were able to derive this lower rainfall limit at which patterned system states cease to exist (see Appendix D).

$$p_{ag} = \frac{m\mu_{p_{ev}} e^{\frac{i_0}{\mu_{p_{ev}}}}}{ca} \tag{14}$$

This is the rainfall value at which desertification occurs: the transition from a vegetated (patterned) state to a bare desert state.

The upper rainfall limit for which patterns exist is equal to the rainfall value at which uniformly vegetated states cease to exist ($p_{ag} \approx 700$ mm yr^{-1} for the current parameter setting), meaning that stable patterned states and stable uniformly vegetated states do not coexist in this model. This can be explained by the absence of a negative effect of areas with high plant biomass on areas with lower plant biomass, as discussed in section 2.5. Since no runon occurs in the interbands, equation (13) reduces to equation (7), meaning these areas behave as if they are uniform system states. If no stable uniformly vegetated state exists ($p_{ag} < 700$ mm yr^{-1}), plant density decays to zero in the interbands directly downhill of the vegetation bands, as in the case of the model run of Figure 3. If, however, a stable uniform vegetated state does exist, plant density no longer decays in the interbands while the uphill parts of the vegetation bands keep propagating in uphill direction. This eventually results in a uniformly vegetated state.

A stable bare desert state exists for the entire parameter range in which patterns can be found. The desert state remains stable up to a rainfall level of $p_{ag} \approx 1070$ mm yr^{-1}. This value, above which revegetation occurs regardless of the amount of biomass introduced, can be obtained analytically (see Appendix D):

$$p_{ag} = \frac{rW^*}{1 - e^{-\frac{i_0}{\mu_{p_{ev}}}}} \tag{15}$$

in which W^* is the resource level at which plant growth equals plant losses [*Tilman*, 1982]: $W^* = \frac{mk}{cu-m}$.

Equations (14) and (15) give the aggregated rainfall rates between which the system can have alternative stable states and where, respectively, desertification and revegetation can be expected to occur. However, we found that desertification may as well occur at a much higher rainfall level than given by equation (14). If the system is in a uniformly vegetated state and rainfall declines over time, a transition to a desert state occurs where uniformly vegetated states cease to exist. Such a transition is not preceded by the formation of vegetation patterns. This system behavior can be attributed to the fact that in our model the patterned states are isolated from the uniform steady states. In most models, patterns arise from a uniformly vegetated state that becomes unstable to heterogeneous perturbations [*Turing*, 1953; *Edelstein-Keshet*, 1988]. As a result, these models predict a sequence of uniform vegetation, patterned vegetation, and desert with increasing aridity. In our model, in contrast, the uniformly vegetated state remains stable and patterns only form if the desert state is perturbed by sufficiently large perturbations. Also notice that, although the bare desert state is stable up to $p_{ag} \approx 1070$mm yr^{-1}, relatively small perturbations are required for revegetation to occur as p_{ag} increases (Figure 4), meaning that bare desert states are unlikely to be observe at such high rainfall values.

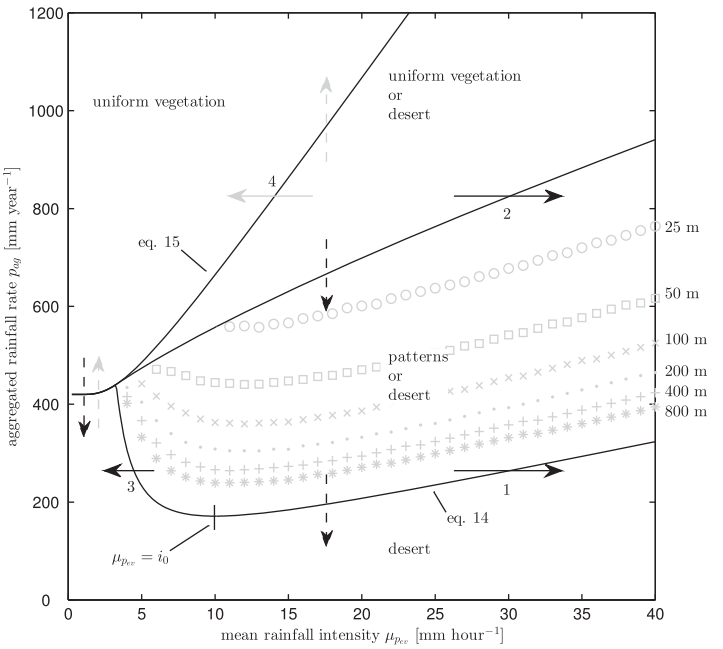

Figure 6. Regions in $(\mu_{p_{ev}}, p_{ag})$–space for which uniform vegetation, patterns, and/or desert states exist. The markers show the lower rainfall limits of patterned states with the indicated wavelengths and were obtained using the bisection method. The arrows indicate how changes in aggregated rainfall rate (dashed) and mean rainfall intensity (solid) can result in a transition to the desert state (black) or in recovery from a desert state (gray). The parameter regions were obtained by plotting equations (14) and (15), as derived in Appendix D. The border between uniform vegetation and patterned vegetation was obtained by finding the minimum of equation (C5). Note that, since rainfall intensity $\mu_{p_{ev}}$ can change while aggregated rainfall p_{ag} remains constant 13, the interarrival time and/or event duration change along the *x* axis, implying that the on the left end of this figure the rainfall is characterized by continuous drizzle, whereas on the right-hand side rainfall consists of sporadic intense events.

3.3. The Response of the Model to Changes in Rainfall Intensity

So far, we have seen that the ability of plants to harvest water depends on rainfall intensity and that during intense rain events an amount of rainwater is lost from the system in the form of runoff (section 3.1). In addition, we found that alternative stable states can coexist, and that the rainfall range for which this occurs depends on mean rainfall intensity (section 3.2). Using equations (14) and (15), we can now study the response of the system to changes in mean rainfall intensity $\mu_{p_{ev}}$. Figure 6 shows that an increase in mean rainfall intensity will widen the rainfall range for which the system has alternative stable system states (this is the case only if $\frac{m}{c} + \frac{rka}{i_0} > u$ as derived in Appendix D). At low mean rainfall intensities, the system does not have alternative stable states and also patterns cannot exist. Short wavelength patterns are most likely to be observed in regions with high mean rainfall intensity. Plants can persist in very dry climates if the mean rainfall intensity is close to the infiltration capacity of bare soil i_0 ($\mu_{p_{ev}} = i_0$ is a minimum of equation (14), see Appendix D) and patterning is most likely to be observed where mean rainfall intensity is higher than the infiltration capacity of bare soil $\mu_{p_{ev}} > i_0$, which is consistent with observations that link vegetation patterns low infiltrability of soils [*Valentin et al.*, 1999].

The response of the system to changes in mean rainfall intensity is affected by model parameters that control infiltration into bare soil i_0 and the impact of plants on soil structure a (Figure 7). The parameters i_0 and a are related to soil type and vegetation composition. The infiltration capacity of sandy soils is generally higher than that of clayey soils, whereas vegetation composed of perennial grasses has a greater impact on soil structure when compared to annual grasses [*Kelly and Walker*, 1976; *Rietkerk et al.*, 2000]. Increasing mean rainfall intensity causes a more pronounced widening of the rainfall range with alternative stable states if the infiltration capacity of bare soil i_0 is low and if the impact of plants on soil structure a is high. Also notice that plants can persist into higher aridity if bare soil infiltration capacity is low and if the impact of plants on soil structure is high.

As indicated by the arrows in Figure 6, changes in mean rainfall intensity can also induce a critical transition to a desert state or cause recovery from a desert state, even if aggregated rainfall rates remain unchanged. If the system is in a patterned state, an increase in mean rainfall intensity can result in desertification (arrow 1 in Figure 6). Such a transition is the result of an increased fraction of events that lead to runoff losses from the hillslope (high intensity events, as defined in section 3.1) and is only possible if the mean rainfall intensity exceeds the infiltration capacity of bare soil. The likelihood that desertification due to increasing mean rainfall intensity occurs is related to the slope of the lower rainfall limit, as given by

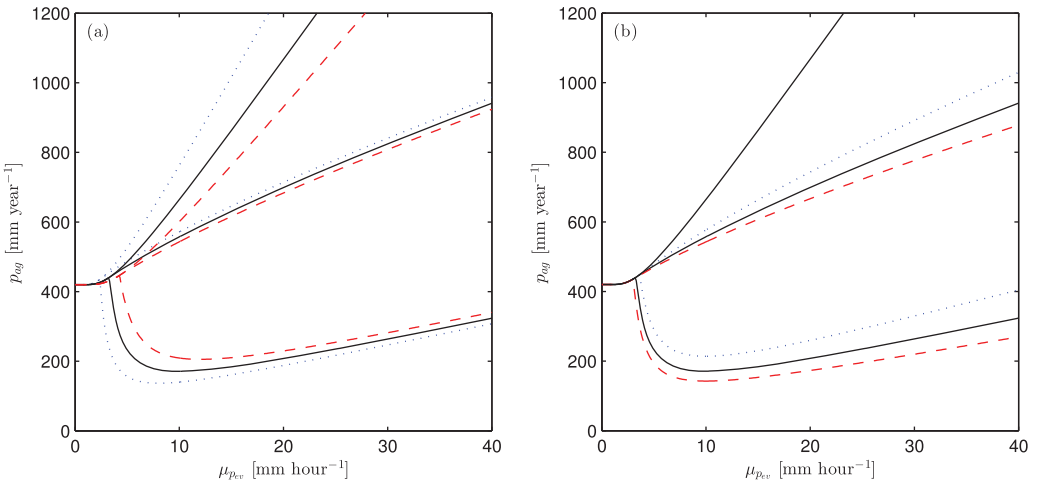

Figure 7. The parameter space as depicted in Figure 6, but now with different values for (a) bare soil infiltration capacity i_0 (mm hr^{-1}) and (b) the increase of infiltration capacity with plant density a (mm m^2 h^{-1} g^{-1}). In Figures 7a and 7b, the black solid curves are the parameter spaces the original parameter values (Table 1). In Figure 7a, the blue dotted curves and the red-dashed curves depict parameter spaces for $i_0 = 8$ mm h^{-1} and $i_0 = 12$ mm h^{-1}, respectively ($\pm$ 20% of the original value). In Figure 7b, the blue dotted curves and the red-dashed curves depict parameter spaces for $a = 1.6$ mm m^2 h^{-1} g^{-1} and $a = 2.4$ mm m^2 h^{-1} g^{-1}, respectively ($\pm$ 20% of the original value).

equation (14), and decreases with impact of plants on soil structure a (see Figure 7). As discussed in the previous section, a transition to a bare desert state can also occur if the system is in a uniformly vegetated state (arrow 2 in Figure 6).

Less intuitive is the fact that a transition to a desert state can result from a decrease in mean rainfall intensity (arrow 3 in Figure 6). This is caused by the fact that a decrease in mean rainfall intensity does not only lead to decreased runoff losses, but also to a lower fraction of events that are intense enough to trigger redistribution of water (intermediate and high intensity events as defined in section 3.1). Consequently, more rainwater infiltrates locally and a greater fraction of the rainwater infiltrates in the bare interbands. As plants are absent in the interbands, this water is eventually lost due to soil evaporation and percolation. Desertification as a result of decreasing rainfall intensity can only occur if the system is in a patterned state (and if $\frac{m}{c} + \frac{rka}{i_0(e-1)} > u$; see Appendix D). If the system is in the desert state, decreasing rainfall intensity can also result in revegetation (if $p_{ag} > rW^*$; arrow 4 in Figure 6).

4. Discussion and Conclusions

In the coming decades, global climate change may affect the functioning of ecosystems in a gradual or sometimes drastic manner. Model studies addressed that semiarid ecosystems can respond in a nonlinear way to changes in variables like grazing and mean annual rainfall [*Noy-Meir*, 1975; *Rietkerk et al*., 1997]. This means that gradual changes can lead to a rapid and significant loss of biological productivity, which is also referred to as desertification. While projections of global climate models are subject to much uncertainty regarding changes in mean annual and seasonal rainfall in arid and semiarid regions, strong trends in rainfall intensity have been reported [*Tebaldi et al*., 2006; *Solomon et al*., 2007]. By combining an ecological model with a simple event based hydrological hillslope model, we were able to study the response of patterned semiarid ecosystems to changes in rainfall intensity.

From analysis of the model, we conclude that projected increases in rainfall intensity can induce and enhance alternative stability of semiarid ecosystems. We found that periodically banded vegetation, resulting from surface water redistribution, cannot exist in regions with low mean rainfall intensity and that these ecosystems are less likely to be alternatively stable. Finally, we found that under certain conditions both an increase and a decrease in mean rainfall intensity can push the system over a critical threshold, resulting in a regime shift to a bare desert state. This finding was attributed to the fact that water can be lost from the system in two ways. During high intensity rain events, a fraction of the water flows through the vegetation

bands and is lost as runoff, while during low intensity events a large portion of the water infiltrates in the bare interbands, where it is not available to plants and eventually lost due to soil evaporation and percolation.

The categorization of rain events into low, intermediate, and high intensity events—as done in this paper to explain the response of the system to changes in mean rainfall intensity—is analogous to field observations by *McDonald et al*. [2009]. In their study on the ecohydrology of banded vegetation patterns in the Chihuahuan Desert (USA), a threshold in storm size was identified above which a part of the runoff from interbands flows through the vegetated bands. In section 3.1, we classified events with an intensity above this threshold as high intensity events. After small rain events wetting depths do not significantly differ between the vegetation bands and the interbands (low intensity events in our classification) [*McDonald et al*., 2009], while during larger storms infiltration in the vegetated bands was significantly higher (intermediate and high intensity events in our classification) [*McDonald et al*., 2009].

Our model differs from other conceptual models in that a (Turing unstable) uniformly vegetated system state and patterned system states do not coexist in our model. This means that patterns cannot form out of uniform vegetation and that if the system is subject to change, a regime shift from a vegetated state to a desert state can occur without a warning in the form of vegetation patterns. We attribute this difference in model behavior to model assumptions that lead to the absence of a negative effect of uphill vegetation on infiltration in the interbands. While we considered infiltration to be limited by the infiltration capacity of a soil, other conceptual models [*HilleRisLambers et al*., 2001; *Rietkerk et al*., 2002; *Gilad et al*., 2004; *Meron et al*., 2007] assume infiltration rates to be controlled by the depth of the surface water layer. Both infiltration models can be justified depending on the type system that is being considered; however, our study indicates that during model development infiltration models should be selected with care, as this choice can fundamentally affect the global behavior of pattern formation models.

The minimalistic modeling approach used in this study enabled us to derive expressions for which the system exhibits alternative stable states and allowed us to derive the conditions required for the occurrence of critical transitions induced by changes in rainfall intensity. However, the choice for an analytically tractable and simplified model may have affected the presented findings in a number of ways.

First, although the model captures the processes of infiltration and surface water redistribution in a hydrologically sensible way, it does not consider the possible interactions between rain events induced by antecedent soil moisture. If the interarrival time between rain events is short, i.e., in climates with frequent rain events (on the left side of Figure 6), soils may be moist at the onset of a rain event leading to decreased infiltration capacities and possibly to enhanced runoff generation. A study by *Baudena et al*. [2007] shows similar mechanisms can lead to decreased productivity of drylands for interarrival times smaller than 3 days. In climates with infrequent high intensity events on the other hand, rainfall induced seal formation may significantly affect soil drying and consequently infiltration [*Assouline and Mualem*, 1997, 2002, 2003].

A second shortcoming of the model is that it does not fully account for the intermittent nature of rainfall, as it does not consider dry down periods and associated vegetation dynamics between rain events. In climates with sporadic high intensity rain events (on the right side of Figure 6), the length of these dry periods may have a great impact on plant mortality, while the effect of infiltration rates on plant growth is of less importance. Model studies show that models that do not consider the intermittent properties of rainfall systematically underestimate the productivity of semiarid ecosystems [*Baudena et al*., 2007; *Baudena and Provenzale*, 2008; *Kletter et al*., 2009]. This underestimation is less pronounced if spatial feedbacks, such as resource redistribution due to infiltration contrasts, govern the system as in our model [*Kletter et al*., 2009; *Baudena and Provenzale*, 2008]. Nonetheless, these effects may still be important if soil water uptake is nonlinear [*Kletter et al*., 2009].

A third issue not accounted for in this study is the fact that the magnitude of variability imposed on the system changes with rainfall intensity. Variability in infiltration rates (see equation (A3) in Appendix A) and soil moisture [see *Rodriguez-Iturbe et al*., 1999] are especially high at intermediate intensities.

Variability in environmental conditions can affect model outcome in various ways. It can cause convergence of the system to a stochastically stable state between the two deterministically stable states [*D'Odorico et al*., 2005], it can result in a shrinkage of the region of bistability [*Guttal and Jayaprakash*, 2007], or it may induce the formation of patterns where one would expect uniform vegetation cover [*D'Odorico et al*., 2006].

Finally, microtopography can play an important role in infiltration and runoff generation. The hydrological part of our model is valid for sheet flow conditions, i.e., the surface water layer is deep compared to the depth of microtopographic depressions. This assumption is justified for sufficiently intense events, but for less intense events surface storage in depressions delays runoff initiation and increases infiltration locally [*Thompson et al*., 2010b]. High intensity events on the other hand, may a trigger changes in geomorphology. This may cause changes in flow patterns and infiltration, and may eventually affect vegetation patterning [*Saco et al*., 2007]. We believe that studying such processes could be done by extending the framework presented here.

Future studies could attempt to verify our findings using areal images. For example, our model suggests that regular patterning only occurs in climatic regions with high mean rainfall intensities. If mean rainfall intensity is indeed a key parameter in explaining regular patterning, it can be used to further improve empirical predictive models such as the one by *Deblauwe et al*. [2008]. Our study also suggests that changes in rainfall intensity may lead to increased resource losses, due to bare soil infiltration and runoff, and that these losses can potentially trigger desertification. Field data could be used to assess the rainfall intensities that separate the different event types as identified in our model study. These values, combined with the frequency distribution of rainfall intensity, can be used to estimate the fractional loss of water from the system in current and future climates, and may thereby help in assessing the proximity of semiarid ecosystems to critical thresholds.

Appendix A: Derivation of First- and Second-Order Moments of Infiltration Rate

Equation (6) is the expected infiltration rate when neglecting runon and is based on equations (3) and (5). The expected infiltration rate can be derived as follows:

$$
\begin{aligned}
\mathrm{E}(i_{ev}) &= \int_0^{\infty} i_{ev} f(p_{ev})\, dp_{ev} \\
&= \int_0^{i_{cap}} p_{ev} f(p_{ev})\, dp_{ev} + \int_{i_{cap}}^{\infty} i_{cap} f(p_{ev})\, dp_{ev} \\
&= \int_0^{i_{cap}} \frac{p_{ev}}{\mu_{p_{ev}}} e^{-\frac{p_{ev}}{\mu_{p_{ev}}}} dp_{ev} + \int_{i_{cap}}^{\infty} \frac{i_{cap}}{\mu_{p_{ev}}} e^{-\frac{p_{ev}}{\mu_{p_{ev}}}} dp_{ev} \\
&= \left[-(\mu_{p_{ev}} + p_{ev}) e^{-\frac{p_{ev}}{\mu_{p_{ev}}}} \right]_0^{i_{cap}} + \left[-i_{cap} e^{-\frac{p_{ev}}{\mu_{p_{ev}}}} \right]_{i_{cap}}^{\infty} \\
&= \mu_{p_{ev}} - (\mu_{p_{ev}} + i_{cap}) e^{-\frac{i_{cap}}{\mu_{p_{ev}}}} + i_{cap} e^{-\frac{i_{cap}}{\mu_{p_{ev}}}} \\
&= \mu_{p_{ev}} \left(1 - e^{-\frac{i_{cap}}{\mu_{p_{ev}}}} \right)
\end{aligned}
\tag{A1}
$$

The expected infiltration rate including runon (equation (12)) is based on equations (5) and (8):

$$
\begin{aligned}
\mathrm{E}(i_{ev}) &= \int_0^{\infty} i_{ev} f(p_{ev}) dp_{ev} \\
&= \int_0^{\tilde{p}_{ev}} p_{ev} f(p_{ev}) dp_{ev} + \int_{\tilde{p}_{ev}}^{\infty} i_{cap} f(p_{ev}) dp_{ev} \\
&= \int_0^{\tilde{p}_{ev}} \frac{p_{ev}}{\mu_{p_{ev}}} e^{-\frac{p_{ev}}{\mu_{p_{ev}}}} dp_{ev} + \int_{\tilde{p}_{ev}}^{\infty} \frac{i_{cap}}{\mu_{p_{ev}}} e^{-\frac{p_{ev}}{\mu_{p_{ev}}}} dp_{ev} \\
&= \left[-(\mu_{p_{ev}} + p_{ev}) e^{-\frac{p_{ev}}{\mu_{p_{ev}}}} \right]_0^{\tilde{p}_{ev}} + \left[-i_{cap} e^{-\frac{p_{ev}}{\mu_{p_{ev}}}} \right]_{\tilde{p}_{ev}}^{\infty} \\
&= \mu_{p_{ev}} - (\mu_{p_{ev}} + \tilde{p}_{ev}) e^{-\frac{\tilde{p}_{ev}}{\mu_{p_{ev}}}} + i_{cap} e^{-\frac{\tilde{p}_{ev}}{\mu_{p_{ev}}}} \\
&= \mu_{p_{ev}} + (i_{cap} - \tilde{p}_{ev} - \mu_{p_{ev}}) e^{-\frac{\tilde{p}_{ev}}{\mu_{p_{ev}}}}
\end{aligned}
\tag{A2}
$$

The variance in infiltration rate is related to the mean rainfall intensity $\mu_{p_{ev}}$ as shown in equation (A3):

$$
\begin{aligned}
\mathrm{VAR}(i_{ev}) &= \int_0^{\infty} (i_{ev} - \mathrm{E}(i_{ev}))^2 f(p_{ev}) dp_{ev} \\
&= \int_0^{i_{cap}} (p_{ev} - \mathrm{E}(i_{ev}))^2 f(p_{ev}) dp_{ev} \\
&\quad + \int_{i_{cap}}^{\infty} (i_{cap} - \mathrm{E}(i_{ev}))^2 f(p_{ev}) dp_{ev} \\
&= \int_0^{i_{cap}} \frac{(p_{ev} - \mathrm{E}(i_{ev}))^2}{\mu_{p_{ev}}} e^{-\frac{p_{ev}}{\mu_{p_{ev}}}} dp_{ev} \\
&\quad + \int_{i_{cap}}^{\infty} \frac{(i_{cap} - \mathrm{E}(i_{ev}))^2}{\mu_{p_{ev}}} e^{-\frac{p_{ev}}{\mu_{p_{ev}}}} dp_{ev} \\
&= \left[-(\mu_{p_{ev}}^2 + (\mathrm{E}(i_{ev}) - \mu_{p_{ev}} - p_{ev})^2) e^{-\frac{p_{ev}}{\mu_{p_{ev}}}} \right]_0^{i_{cap}} \\
&\quad + \left[-(i_{cap} - \mathrm{E}(i_{ev}))^2 e^{-\frac{p_{ev}}{\mu_{p_{ev}}}} \right]_{i_{cap}}^{\infty} \\
&= \mu_{p_{ev}}^2 + (\mathrm{E}(i_{ev}) - \mu_{p_{ev}})^2 \\
&\quad + 2\mu_{p_{ev}} (\mathrm{E}(i_{ev}) - \mu_{p_{ev}} - i_{cap}) e^{-\frac{i_{cap}}{\mu_{p_{ev}}}} \\
&= \mu_{p_{ev}} \left(\mu_{p_{ev}} - 2i_{cap} e^{-\frac{i_{cap}}{\mu_{p_{ev}}}} - \mu_{p_{ev}} e^{-2\frac{i_{cap}}{\mu_{p_{ev}}}} \right)
\end{aligned}
\tag{A3}
$$

For $0 < \mu_{p_{ev}} \ll i_{cap}$, the variance increases quadratically with $\mu_{p_{ev}}$. The variance in infiltration rate reaches a maximum at $\mu_{p_{ev}} \approx 0.89 i_{cap}$, after which it slowly declines with increasing rainfall intensity. A similar response can be found in soil moisture variance [*Rodriguez-Iturbe et al*., 1999] which is not only determined by the mean rainfall depth (the product of rainfall intensity and duration) but also by the interarrival time or frequency of the rain events and soil water losses.

Appendix B: Feedbacks Between Vegetation Bands and Interbands if Infiltration Is Depth Dependent

In the model presented in this paper, the infiltration rate is independent of surface water depth. In most models that generate patterns and that account for a surface water-related pattern forming mechanism, infiltration rate is (linearly) related to surface water depth. An equation commonly used in conceptual models is given by *HilleRisLambers et al*. [2001], *Rietkerk et al*. [2002], *Gilad et al*. [2004], and *Meron et al*. [2007]:

$$I(O,P) = \alpha O \frac{P + kW_0}{P + k} \tag{B1}$$

Here I is the infiltration rate, α is the maximum infiltration rate, O is the surface water depth, P is the plant density, k is a half saturation constant, and W_0 is the fraction of water that infiltrates in absence of plants.

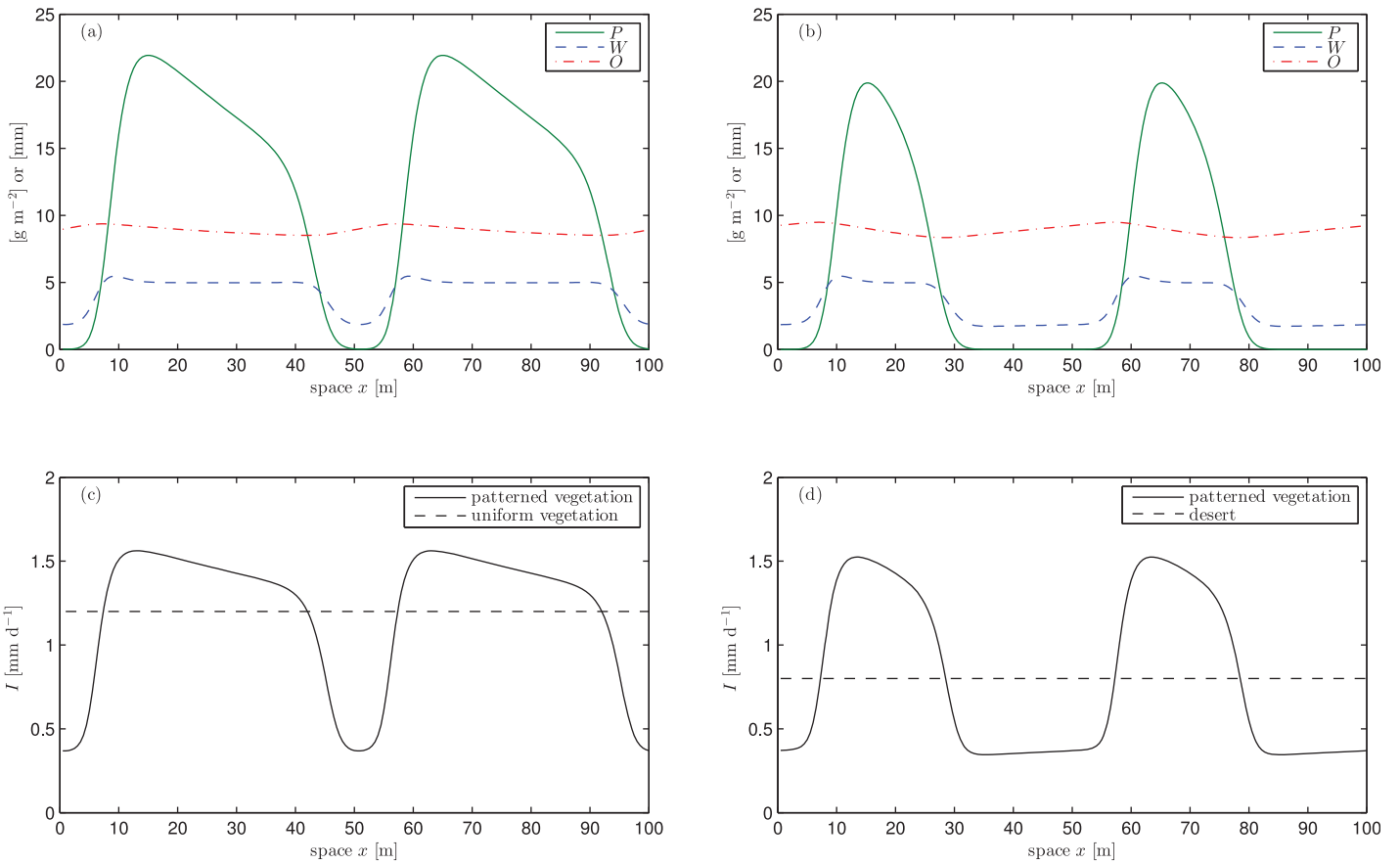

Figure B1. (a and b) Surface water O (mm), soil water W (mm), and plant density P (g m^{-2}) along a hillslope generated using a one-dimensional version of the model by *Rietkerk et al*. [2002] with mortality rate $d = 0.25$ d^{-1}, downhill flow rate $v = 10$ m d^{-1}, and surface water diffusion $D_O = 0$ m^2 d^{-1}. In Figure B1a, rainfall rate $R = 1.2$ mm d^{-1} and in Figure B1b $R = 0.8$ mm d^{-1}. Surface water flows from left to right. (c and d) Infiltration rate I (mm d^{-1}) for the patterned states of Figures B1a and B1b (solid line) and for uniform states (dashed line).

Modeling infiltration with surface water depth dependence, as in equation (B1), results in a negative effect of the vegetation bands on the bare interbands because surface water is depleted in the vegetation bands and consequently surface water depth is lower downhill of vegetation bands (see Figures B1a and B1b). As a result, infiltration rate in the interbands is lower than in absence of vegetation bands as shown in Figures B1c and B1d.

Appendix C: Bifurcation Diagram

The equilibria shown in Figure 4 can be derived by setting equations (1) and (2) to zero and neglecting diffusion terms $d_W \frac{\partial^2 W}{\partial x^2} = d_P \frac{\partial^2 P}{\partial x^2} = 0$:

$$\frac{\partial W}{\partial t} = i_{ag} - u\frac{W}{W+k}P - rW = 0 \tag{C1}$$

$$\frac{\partial P}{\partial t} = cu\frac{W}{W+k}P - mP = 0 \tag{C2}$$

Solving gives:

$$\frac{\partial W}{\partial t} = 0 \text{ at :}$$
$$W = \frac{i_{ag} - uP - rk \pm \sqrt{(uP + rk - i_{ag})^2 + 4rki_{ag}}}{2r} \tag{C3}$$

$$\frac{\partial P}{\partial t} = 0 \text{ at :}$$
$$P = 0 \text{ and } W^* = \frac{mk}{cu - m} \tag{C4}$$

By plotting solutions (C3) and (C4) with $\tilde{p}_{ev} = i_{cap}$, we obtain the phase planes for the homogeneous system shown in Figure C1. The stability and the number of system states change with aggregated rainfall rate p_{ag}. The behavior of the system is very similar to the original model by *Rietkerk et al.* [1997]. The isocline of soil water availability losses its humped shape if rainfall intensity is low, meaning that the transition from and to a bare desert state becomes supercritical (see Figure 6).

The uniform steady states depicted in Figure 4a were obtained by writing aggregated rainfall as a function of plant density:

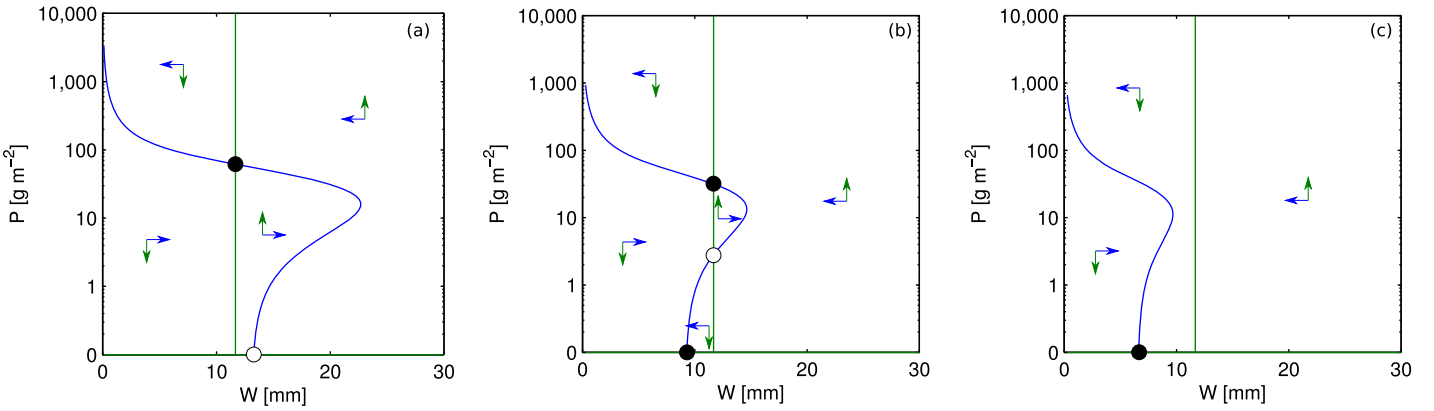

Figure C1. Phase planes with (a) $p_{ag} = 1200$, (b) $p_{ag} = 840$, and (c) $p_{ag} = 600$ mm yr^{-1} for uniform conditions ($d_W \frac{\partial^2 W}{\partial x^2} = d_P \frac{\partial^2 P}{\partial x^2} = 0$ and $\tilde{p}_{ev} = i_{cap}$). In blue, the isocline of available soil water ($\frac{dW}{dt} = 0$, equation (C3)). In green, the isoclines of plant density ($\frac{dP}{dt} = 0$, equation (C4)). The system is in equilibrium if $\frac{dW}{dt} = \frac{dP}{dt} = 0$, i.e., where the isoclines intersect. Open circles indicate unstable equilibria and closed circles indicate stable equilibria. The vectors show the direction of change if the system is out of equilibrium.

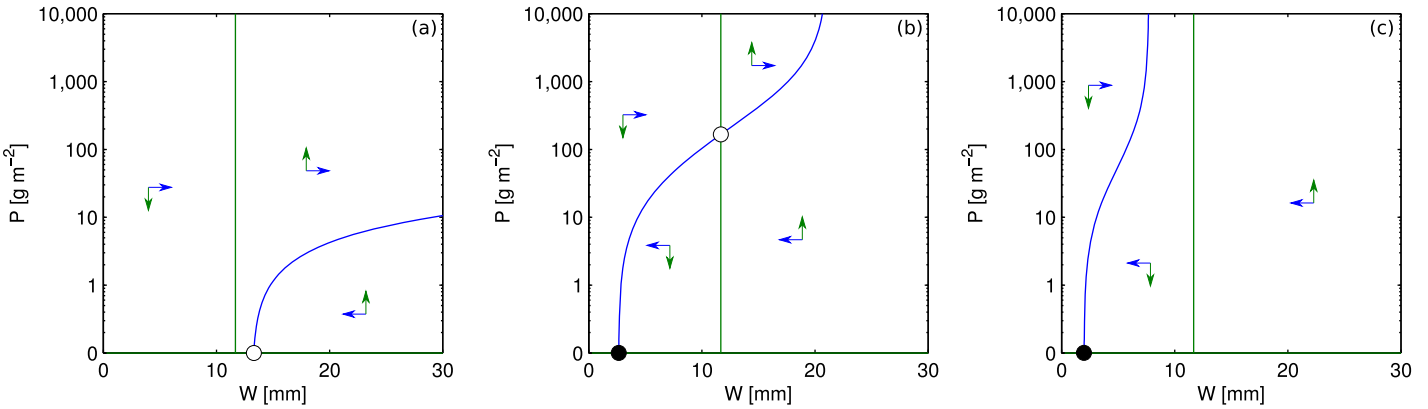

Figure C2. See caption of Figure C1 but with (a) $p_{ag} = 1200$, (b) $p_{ag} = 240$, and (c) $p_{ag} = 180$ mm yr^{-1}. Now $\tilde{p}_{ev} = i_0$ and P reflects the plant density in a vegetation band. Notice that plant density either decreases to zero or increases to infinity. The latter is due to the fact that we neglect diffusion losses $\left(d_W \frac{\partial^2 W}{\partial x^2} = d_P \frac{\partial^2 P}{\partial x^2} = 0\right)$ that, in the full model, would slow down plant growth as plant density increases.

$$p_{ag} = \frac{\frac{m}{c}P + rW^*}{1 - e^{-\frac{i_0 + aP}{\mu_{pev}}}} \tag{C5}$$

The minimum plant density needed for plants to grow or sustain in Figure 4b is basically an unstable equilibrium above which the plant density in a vegetation band on an infinitely long bare hillslope increases. The soil uphill of the vegetation band is bare; therefore, runon will occur if $p_{ev} > i_0$, meaning that the critical rainfall intensity $\tilde{p}_{ev}$ can be assumed to equal the infiltration capacity of bare soil i_0. Since the hillslope is assumed to be infinitely long, runon occurs along the full width of the vegetation band. We again need to neglect losses of soil water and plant density due to diffusion $d_W \frac{\partial^2 W}{\partial x^2} = d_P \frac{\partial^2 P}{\partial x^2} = 0$, meaning that the vegetation band needs to be sufficiently wide so that in its center diffusion losses approach zero. The phase planes depicted in Figure C2 can again be obtained by plotting solutions (C3) and (C4), but now with $\tilde{p}_{ev} = i_0$.

The curve of minimum plant density required for recovery as depicted in Figure 4 was obtained by writing aggregated rainfall as a function of plant density:

$$p_{ag} = \frac{\frac{m}{c}P + rW^*}{1 + \left(\frac{aP}{\mu_{pev}} - 1\right)e^{-\frac{i_0}{\mu_{pev}}}} \tag{C6}$$

Appendix D : Region With Alternative Stable System States

D1. Upper Rainfall Limit

Equation (D1) (equation (15) in main text) gives the highest value of p_{ag} for which the system has multiple stable system states (upper line in Figure 6b). Here the bare desert state changes stability: the isoclines for available soil water and plant density intersect at $P = 0$. Equation (D1) can be obtained by filling in $P = 0$ in equation (C5):

$$p_{ag} = \frac{rW^*}{1 - e^{-\frac{i_0}{\mu_{pev}}}} \tag{D1}$$

The derivative of equation (D1) with respect to mean rainfall intensity $\mu_{p_{ev}}$ is given by:

$$\frac{dp_{ag}}{d\mu_{p_{ev}}} = \frac{i_0 rW^* e^{\frac{i_0}{\mu_{pev}}}}{\mu_{p_{ev}}^2 \left(e^{\frac{i_0}{\mu_{pev}}} - 1\right)^2} \tag{D2}$$

Given that $W^* > 0$ and that all parameter values are positive, $\frac{dp_{ag}}{d\mu_{p_{ev}}} > 0$. This means that the aggregated rainfall required for recovery from the desert state increases with rainfall intensity.

As the mean rainfall intensity $\mu_{p_{ev}}$ increases, equation (D1) approaches a asymptote with a constant slope:

$$\left.\frac{dp_{ag}}{d\mu_{p_{ev}}}\right|_{\mu_{p_{ev}}\to\infty} = \frac{rW^*}{i_0} \tag{D3}$$

D2. Lower Rainfall Limit

Assuming that stable (patterned) states exists as long as the plant density required to recover from the bare state is finite, the lower limit of the region with alternative stable system states is given by equation (D4) (equation (14) in main text). This is the aggregated rainfall rate p_{ag} that is approached as $P \to \infty$ in equation (C6):

$$p_{ag} = \frac{m\mu_{p_{ev}} e^{\frac{i_0}{\mu_{p_{ev}}}}}{ca} \tag{D4}$$

The derivative of equation (D4) with respect to mean rainfall intensity $\mu_{p_{ev}}$ is given by:

$$\frac{dp_{ag}}{d\mu_{p_{ev}}} = \frac{m(\mu_{p_{ev}} - i_0)e^{\frac{i_0}{\mu_{p_{ev}}}}}{ca\mu_{p_{ev}}} \tag{D5}$$

Equation (D5) is positive if $\mu_{p_{ev}} > i_0$ and negative if $\mu_{p_{ev}} < i_0$. A minimum of equation (D4) can be found at $\mu_{p_{ev}} = i_0$. As the rainfall intensity $\mu_{p_{ev}}$ increases, equation (D4) approaches an asymptote with slope:

$$\left.\frac{dp_{ag}}{d\mu_{p_{ev}}}\right|_{\mu_{p_{ev}}\to\infty} = \frac{m}{ca} \tag{D6}$$

D3. Robustness of the Presented Model Results

In the main text (section 3.3), we state that if the aggregated rainfall rate remains unchanged, then both an increase and a decrease in mean rainfall intensity can result in desertification. In addition, we claim that the width of the bistable region, in terms of aggregated rainfall, increases with mean rainfall intensity. These findings hold for the parameter combination listed in Table 1 as shown in Figure 6. Here we study the robustness of these findings: what are parameter combinations are required for these findings to be valid?

Assuming that the transition from a patterned state to a desert state occurs at an aggregated rainfall rate given by equation (D4), both an increase and a decrease in mean rainfall intensity can result in desertification, only if the second derivative of equation (D4) with respect to $\mu_{p_{ev}}$ in $\mu_{p_{ev}} = i_0$ is positive:

$$\left.\frac{d^2p_{ag}}{d\mu_{p_{ev}}^2}\right|_{\mu_{p_{ev}}=i_0} = \frac{me}{i_0ac} > 0 \tag{D7}$$

This is always true since all parameter values are positive. Desertification induced by declining mean rainfall intensity can only occur if the desert state is stable at this minimum. Filling in $\mu_{p_{ev}} = i_0$ in equations (D1) and (D4) results in the following condition:

$$\frac{rW^*}{1-e^{-1}} > \frac{mi_0e}{ca} \tag{D8}$$

Rewriting gives:

$$\frac{m}{c} + \frac{rka}{i_0(e-1)} > u \tag{D9}$$

The region of bistability, in terms of aggregated rainfall, increases with mean rainfall intensity. This is always true for $\mu_{p_{ev}} \leq i_0$, since here the slope of the lower rainfall limit (equation (D5)) is negative while the slope

of the upper rainfall limit is positive (equation (D2)). From equations (D3) and (D6) follows that for high values of mean rainfall intensity, the bistable region increases with mean rainfall intensity if:

$$\frac{rW^*}{i_0} > \frac{m}{ca} \tag{D10}$$

Rewriting yields:

$$\frac{m}{c} + \frac{rka}{i_0} > u \tag{D11}$$

Acknowledgments
We thank Eric Siero, Arjen Doelman, and Jens Rademacher for the fruitful discussions we had on the topic of patterning in semiarid ecosystems. This study is supported by a grant within the Complexity program of the Netherlands Organization of Scientific Research (NWO). The research of MB and MR is also supported by funding from the European Union's Seventh Framework Programme (FP7/2007–2013) under grant 283068 (CASCADE).

References

Assouline, S., and Y. Mualem (1997), Modeling the dynamics of seal formation and its effect on infiltration as related to soil and rainfall characteristics, *Water Resour. Res.*, *33*(7), 1527–1536.
Assouline, S., and Y. Mualem (2002), Infiltration during soil sealing: The effect of areal heterogeneity of soil hydraulic properties, *Water Resour. Res.*, *38*(12), 1286, 22–1–22-9, doi:10.1029/2001WR001168.
Assouline, S., and Y. Mualem (2003), Effect of rainfall-induced soil seals on the soil water regime: Drying interval and subsequent wetting, *Transp. Porous Media*, *53*(1), 75–94.
Baudena, M., and A. Provenzale (2008), Rainfall intermittency and vegetation feedbacks in drylands, *Hydrol. Earth Syst. Sci.*, *12*, 679–689.
Baudena, M., G. Boni, L. Ferraris, J. von Hardenberg, and A. Provenzale (2007), Vegetation response to rainfall intermittency in drylands: Results from a simple ecohydrological box model, *Adv. Water Resour.*, *30*(5), 1320–1328, doi:10.1016/j.advwatres.2006.11.006.
Bierkens, M., and C. Puente (1990), Analytically derived runoff models based on rainfall point processes, *Water Resour. Res.*, *26*(11), 2653–2659.
Borgogno, F., P. D'Odorico, F. Laio, and L. Ridolfi (2009), Mathematical models of vegetation pattern formation in ecohydrology, *Rev. Geophys.*, *47*, RG1005, 1–36, doi:10.1029/2007RG000256.
Burden, R. L., and J. D. Faires (2011), The bisection method, in *Numerical Analysis*, edited by M. Julet, M. Taylor, and D. Seibert, chap. 2.1, pp. 48–56, Brooks/Cole, Boston, Mass.
DeAngelis, D. L., W. M. Post, and C. C. Travis (1980), *Positive Feedback in Natural Systems*, 290 pp., Springer, Berlin.
Deblauwe, V., N. Barbier, P. Couteron, O. Lejeune, and J. Bogaert (2008), The global biogeography of semi-arid periodic vegetation patterns, *Global Ecol. Biogeogr.*, *17*(6), 715–723, doi:10.1111/j.1466–8238.2008.00413.x.
Deblauwe, V., P. Couteron, O. Lejeune, J. Bogaert, and N. Barbier (2011), Environmental modulation of self-organized periodic vegetation patterns in Sudan, *Ecography*, *34*(6), 990–1001, doi:10.1111/j.1600-0587.2010.06694.x.
Deblauwe, V., P. Couteron, J. Bogaert, and N. Barbier (2012), Determinants and dynamics of banded vegetation pattern migration in arid climates, *Ecol. Monogr.*, *82*(1), 3–21.
D'Odorico, P., F. Laio, and L. Ridolfi (2005), Noise-induced stability in dryland plant ecosystems, *Proc. Natl. Acad. Sci. U. S. A.*, *102*(31), 10,819–10,822, doi:10.1073/pnas.0502884102.
D'Odorico, P., F. Laio, and L. Ridolfi (2006), Vegetation patterns induced by random climate fluctuations, *Geophys. Res. Lett.*, *33*, L19404, doi:10.1029/2006GL027499.
D'Odorico, P., A. Bhattachan, K. F. Davis, S. Ravi, and C. W. Runyan (2013), Global desertification: Drivers and feedbacks, *Adv. Water Resour.*, *51*, 326–344, doi:10.1016/j.advwatres.2012.01.013.
Dunkerley, D. L. (2013), Vegetation mosaics of arid Western New South Wales, Australia: Considerations of their origin and persistence, in *Patterns of Land Degradation in Drylands; Understanding Self-Organised Ecogeomorphic Systems*, edited by E. N. Mueller, J. Wainwright, A. J. Parsons, and L. Turnbull, edition 1, pp. 315–345, Springer, Dordrecht.
Dunne, T., W. Zhang, and B. Aubry (1991), Effects of rainfall, vegetation, and microtopography on infiltration and runoff, *Water Resour. Res.*, *27*(9), 2271–2285.
Edelstein-Keshet, L. (1988), *Mathematical Models in Biology*, 586 pp., McGraw-Hill, N. Y.
Fox, D., Y. Le Bissonnais, and A. Bruand (1998), The effect of ponding depth on infiltration in a crusted surface depression, *Catena*, *32*(2), 87–100, doi:10.1016/S0341–8162(98)00042-3.
Gierer, A., and H. Meinhardt (1972), A theory of biological pattern formation, *Kybernetik*, *12*(1), 30–39.
Gilad, E., J. von Hardenberg, A. Provenzale, M. Shachak, and E. Meron (2004), Ecosystem engineers: From pattern formation to habitat creation, *Phys. Rev. Lett.*, *93*(9), 1–4, doi:10.1103/PhysRevLett.93.098105.
Guttal, V., and C. Jayaprakash (2007), Impact of noise on bistable ecological systems, *Ecol. Modell.*, *201*(3–4), 420–428, doi:10.1016/j.ecolmodel.2006.10.005.
HilleRisLambers, R., M. Rietkerk, F. V. D. Bosch, H. H. T. Prins, and H. D. Kroon (2001), Vegetation pattern formation in semi-arid grazing systems, *Ecology*, *82*(1), 50–61.
Hoogmoed, W. B. (1981), Analysis of rainfall in some locations of West Africa and India, in *Development of Criteria and Methods for Improving the Efficiency of Soil Management and Tillage Operations, With Special Reference to Arid and Semi-Arid Regions*, edited by E. Rawitz, W. B. Hoogmoed, and Y. Morin, 260 pp., Hebrew Univ. of Jerusalem, Jerusalem.
Horton, R. E. (1939), Analysis of runoff-plot experiments with varying infiltration-capacity, *Trans. Am. Geophys. Union*, *20*(4), 693–711, doi:10.1029/TR020i004p00693.
Jones, C., J. Lawton, and M. Shachak (1994), Organisms as ecosystem engineers, *Oikos*, *69*, 373–386.
Karssenberg, D. (2006), Upscaling of saturated conductivity for Hortonian runoff modelling, *Adv. Water Resour.*, *29*(5), 735–759, doi:10.1016/j.advwatres.2005.06.012.
Kéfi, S., M. Rietkerk, C. L. Alados, Y. Pueyo, V. P. Papanastasis, A. Elaich, and P. C. de Ruiter (2007), Spatial vegetation patterns and imminent desertification in Mediterranean arid ecosystems, *Nature*, *449*(7159), 213–217, doi:10.1038/nature06111.
Kéfi, S., M. B. Eppinga, P. C. Ruiter, and M. Rietkerk (2010), Bistability and regular spatial patterns in arid ecosystems, *Theor. Ecol.*, *3*(4), 257–269, doi:10.1007/s12080-009-0067-z.

Kelly, R., and B. Walker (1976), The effects of different forms of land use on the ecology of a semi-arid region in south-eastern Rhodesia, *J. Ecol.*, *64*(2), 553–576.
Klausmeier, C. A. (1999), Regular and irregular patterns in semiarid vegetation, *Science*, *284*(5421), 1826–1828.
Kletter, A., J. von Hardenberg, E. Meron, and A. Provenzale (2009), Patterned vegetation and rainfall intermittency, *J. Theor. Biol.*, *256*(4), 574–583, doi:10.1016/j.jtbi.2008.10.020.
Konings, A. G., S. C. Dekker, M. Rietkerk, and G. G. Katul (2011), Drought sensitivity of patterned vegetation determined by rainfall-land surface feedbacks, *J. Geophys. Res.*, *116*, G04008, doi:10.1029/2011JG001748.
Lefever, R., and O. Lejeune (1997), On the origin of tiger bush, *Bull. Math. Biol.*, *59*(2), 263–294.
Lejeune, O., M. Tlidi, and R. Lefever (2004), Vegetation spots and stripes: Dissipative structures in arid landscapes, *Int. J. Quant. Chem.*, *98*(2), 261–271, doi:10.1002/qua.10878.
Lewontin (1969), The meaning of stability, *Brookhaven Symp. Biol.*, *22*, 13–24.
McDonald, A., R. Kinucan, and L. Loomis (2009), Ecohydrological interactions within banded vegetation in the northeastern Chihuahuan Desert, USA, *Ecohydrology*, *2*, 66–71, doi:10.1002/eco.
McGrath, G. S., K. Paik, and C. Hinz (2012), Microtopography alters self-organized vegetation patterns in water-limited ecosystems, *J. Geophys. Res.*, *117*, G03021, doi:10.1029/2011JG001870.
Meron, E., H. Yizhaq, and E. Gilad (2007), Localized structures in dryland vegetation: Forms and functions, *Chaos*, *17*(3), 037109, doi:10.1063/1.2767246.
Novak, V., J. Šimůnek, and M. Genuchten (2000), Infiltration of water into soil with cracks, *J. Irrig. Drain. Eng.*, *126*, 41–47.
Noy-Meir, I. (1975), Stability of grazing systems: An application of predator-prey graphs, *J. Ecol.*, *63*(2), 459–481.
Penny, G. G., K. E. Daniels, and S. E. Thompson (2013), Local properties of patterned vegetation: Quantifying endogenous and exogenous effects, *Philos. Trans. R. Soc. A*, *371*(2004), 20120359.
Philip, J. (1957), The theory of infiltration. 1: The infiltration equation and its solution, *Soil Sci.*, *83*, 345–357.
Rietkerk, M. (1998), Catastrophic vegetation dynamics and soil degradation in semi-arid grazing systems, PhD thesis, Landbouwhogeschool Wageningen, Netherlands.
Rietkerk, M., and J. van de Koppel (2008), Regular pattern formation in real ecosystems, *Trends Ecol. Evol.*, *23*(3), 169–75, doi:10.1016/j.tree.2007.10.013.
Rietkerk, M., F. van den Bosch, and J. van de Koppel (1997), Site-specific properties and irreversible vegetation changes in semi-arid grazing systems, *Oikos*, *80*, 241–252.
Rietkerk, M., P. Ketner, J. Burger, B. Hoorens, and H. Olff (2000), Multiscale soil and vegetation patchiness along a gradient of herbivore impact in a semi-arid grazing system in West Africa, *Plant Ecol.*, *148*, 207–224.
Rietkerk, M., M. C. Boerlijst, F. V. Langevelde, R. Hillerislambers, J. Van, D. Koppel, L. Kumar, H. H. T. Prins, and M. D. Roos (2002), Self-Organization of Vegetation in Arid Ecosystems, *Am. Nat.*, *160*(4), 524–530.
Rietkerk, M., S. C. Dekker, P. C. de Ruiter, and J. van de Koppel (2004), Self-organized patchiness and catastrophic shifts in ecosystems, *Science*, *305*(5692), 1926–1929, doi:10.1126/science.1101867.
Rodriguez-Iturbe, I., A. Porporato, L. Ridolfi, V. Isham, and D. R. Coxi (1999), Probabilistic modelling of water balance at a point: The role of climate, soil and vegetation, *Proc. R. Soc. A*, *455*(1990), 3789–3805, doi:10.1098/rspa.1999.0477.
Saco, P. M., G. R. Willgoose, and G. R. Hancock (2007), Eco-geomorphology of banded vegetation patterns in arid and semi-arid regions, *Hydrol. Earth Syst. Sci.*, *11*(6), 1717–1730, doi:10.5194/hess-11-1717-2007.
Schlesinger, W. H., J. F. Reynolds, G. L. Cunningham, L. F. Huenneke, W. M. Jarrell, R. A. Virginia, and W. G. Whitford (1990), Biological feedbacks in global desertification, *Science*, *247*(4946), 1043–1048.
Sherratt, J. A. (2013), History-dependent patterns of whole ecosystems, *Ecol. Complex.*, *14*, 8–20, doi:10.1016/j.ecocom.2012.12.002.
Sherratt, J. A., and G. J. Lord (2007), Nonlinear dynamics and pattern bifurcations in a model for vegetation stripes in semi-arid environments, *Theor. Popul. Biol.*, *71*(1), 1–11, doi:10.1016/j.tpb.2006.07.009.
Solomon, S., D. Qin, M. Manning, Z. Chen, M. Marquis, K. B. Averyt, M. Tignor, and H. L. Miller (2007), *IPCC, 2007: Climate Change 2007: The Physical Science Basis. Contribution of Working Group I to the Fourth Assessment Report of the Intergovernmental Panel on Climate Change, Geneva*, 996 pp., Cambridge Univ. Press, Cambridge, U. K.
Tebaldi, C., K. Hayhoe, J. M. Arblaster, and G. A. Meehl (2006), Going to the extremes, *Clim. Change*, *79*(3–4), 185–211, doi:10.1007/s10584-006-9051-4.
Thompson, S., and G. Katul (2009), Secondary seed dispersal and its role in landscape organization, *Geophys. Res. Lett.*, *36*, L02402, doi:10.1029/2008GL036044.
Thompson, S., G. Katul, A. Konings, and L. Ridolfi (2011), Unsteady overland flow on flat surfaces induced by spatial permeability contrasts, *Adv. Water Resour.*, *34*(8), 1049–1058, doi:10.1016/j.advwatres.2011.05.012.
Thompson, S. E., C. J. Harman, P. Heine, and G. G. Katul (2010a), Vegetation-infiltration relationships across climatic and soil type gradients, *J. Geophys. Res.*, *115*, G02023, doi:10.1029/2009JG001134.
Thompson, S. E., G. G. Katul, and A. Porporato (2010b), Role of microtopography in rainfall-runoff partitioning: An analysis using idealized geometry, *Water Resour. Res.*, *46*, W07520, doi:10.1029/2009WR008835.
Tilman, D. (1982), Resource competition and community structure, *Monogr. Popul. Biol.*, *17*, 1–296.
Turing, A. (1953), The chemical basis of morphogenesis, *Bull. Math. Biol.*, *237*, 37–72.
Ursino, N., and S. Contarini (2006), Stability of banded vegetation patterns under seasonal rainfall and limited soil moisture storage capacity, *Adv. Water Resour.*, *29*(10), 1556–1564, doi:10.1016/j.advwatres.2005.11.006.
Valentin, C., J. D'Herbès, and J. Poesen (1999), Soil and water components of banded vegetation patterns, *Catena*, *37*(1–2), 1–24, doi:10.1016/S0341-8162(99)00053-3.
van de Koppel, J., and C. M. Crain (2006), Scale-dependent inhibition drives regular tussock spacing in a freshwater marsh, *Am. Nat.*, *168*(5), E136–E147, doi:10.1086/508671.
van Wijngaarden, W. (1985), Elephants Trees Grass Grazers; relationships between climate, soil, vegetation and large herbivores in a semi-arid savanna ecosystem (Tsavo, Kenya), PhD thesis, Landbouwhogeschool Wageningen, Netherlands.
Von Hardenberg, J., E. Meron, M. Shachak, and Y. Zarmi (2001), Diversity of vegetation patterns and desertification, *Phys. Rev. Lett.*, *87*(19), 3–6, doi:10.1103/PhysRevLett.87.198101.
Worrall, G. (1959), The Butana grass patterns, *J. Soil Sci.*, *10*(1), 34–53.
Yizhaq, H., E. Gilad, and E. Meron (2005), Banded vegetation: Biological productivity and resilience, *Physica A*, *356*(1), 139–144, doi:10.1016/j.physa.2005.05.026.